International Journal of Technology

http://ijtech.eng.ui.ac.id

Research Article

Comparative Acoustic Emission Signature Analysis of Magnesium and Steel in Microblanking Process Using Wavelet Scattering Transform

Siska Titik Dwiyati[1], Irwan Setyanto[1], Gandjar Kiswanto[1*], Sugeng Supriadi[1], Tegoeh Tjahjowidodo[2]

[1]Department of Mechanical Engineering, Universitas Indonesia, Depok, West Java, 16424, Indonesia

[2]Department of Mechanical Engineering, KU Leuven, Sint-Katelijne-Waver, 2860, Belgium

[*]Corresponding author: gandjar_kiswanto@eng.ui.ac.id

Abstract: Real-time defect detection is essential for advanced in-process quality inspection systems, particularly for identifying complex crack formations in small-scale products through automated methods. Acoustic emission (AE) enables the rapid detection of crack initiation, making it a highly effective technique for modern manufacturing processes. This study presents a comparative analysis of AE signatures generated during the microblanking process of magnesium and SK-5 steel. Experiments were conducted using a proprietary 5 kN micro-forming machine on 0.1-mm-thick SK-5 steel and 0.5-mm-thick magnesium plates, representing materials with contrasting mechanical properties. This study evaluates and compares various signal processing methods, including the fast Fourier transform (FFT) and the wavelet scattering transform (WST), in terms of their effectiveness in identifying crack initiation events. The wavelet scattering transform exhibited enhanced sensitivity for detecting crack initiation in both materials, with distinct signature patterns identified between the magnesium and SK-5 steel specimens. However, there were limitations for softer materials or when the original signal amplitude was lower than the system noise level. Overall, this comparative analysis provides valuable insights for developing material-specific acoustic emission monitoring systems for microforming applications.

Keywords: Acoustic emission; Crack monitoring; Microforming; Wavelet scattering

1. Introduction

Metal forming technology remains a fundamental manufacturing process for producing precision components across industries despite its long history. Its significance lies in the ability to produce high-quality, dimensionally accurate parts under tightly controlled conditions. Forming processes are classified based on their working principles and are influenced by factors such as material type, billet geometry, temperature, and stress-strain conditions (Li and Fu, 2019; Altan and Tekkaya, 2012). The growing demand for lightweight and high-performance components with complex geometries, particularly those made from materials that are difficult to deform, has driven the development of advanced forming technologies and energy-assisted processes Li and Fu, 2019. However, as materials and geometries become increasingly complex, the risk of defects during processing also increases. Effective defect detection and control have become critical challenges in modern manufacturing (Sutherland et al., 2020; Allwood et al., 2013; Ingarao et al., 2011).

Multiple factors influence defect formation, including material properties, process parameters, and component design. Such defects may occur in various forms, locations, and scales Li and Fu, 2019, compromising dimensional accuracy, mechanical performance, and functional reliability Ma et al., 2025. These defects can lead to tool failure, machine downtime, increased energy consumption, and material waste in severe cases.

https://doi.org/10.14716/ijtech.v17i3.8115
Received September 2025; Revised November 2025; Accepted April 2026

Real-time monitoring techniques have advanced significantly to address these issues. While direct inspection methods benefit macro-scale components, micro-scale forming relies heavily on acoustic emission analysis. AE results from transient elastic waves generated by the rapid release of strain energy during plastic deformation, crack initiation, or phase transformations. These waves propagate through the material and can be detected by sensitive piezoelectric sensors, enabling the identification of internal structural changes in real-time. AE not only enables defect detection but also facilitates the assessment of material behaviour and structural integrity under loading (Mu et al., 2022; Zhang et al., 2020), making it particularly suitable for monitoring microcrack propagation in challenging forming processes (Alcaraz et al., 2024; Zhang and Lin, 2023; Xu et al., 2022; Seleznev et al., 2022).

In modern manufacturing, product quality is a key factor influencing sustainability, cost efficiency, and competitiveness (Kumar et al., 2018; Nurcahyo et al., 2019). Sustainable production requires continuous quality monitoring and data logging for effective process optimization. In microforming, which is used to produce miniature near-net-shape components for medical devices, electronics, and sensors, AE-based systems offer an effective solution. As a non-destructive testing (NDT) method, AE enables in-process monitoring, unlike post-process techniques such as X-ray or ultrasonic testing (Abdollahi-Mamoudan et al., 2025).

A progressive micro-forming process can reduce the challenges associated with handling and removing micro-parts (Ghassemali et al., 2012), as it enhances productivity by integrating multiple operations into a single press cycle. However, defect detection prior to subsequent stages is crucial, particularly when processing brittle materials such as magnesium, which exhibit low ductility at room temperature (Dwiyati et al., 2025) and rapid crack propagation (Wang et al., 2022). AE has proven to be effective for monitoring complex materials, including anisotropic magnesium alloys (Shiraiwa et al., 2019), TRIP/TWIP steels (Linderov et al., 2014), and composites (Al-Jumaili et al., 2018; Barile et al., 2020). In addition, AE has been studied for tool condition monitoring (Twardowski et al., 2021; Unterberg et al., 2021). Nevertheless, the stochastic nature of AE signals, which are sensitive to microstructural features such as grain size, dislocation activity, and inclusions, remains a challenge (Ono, 2005; Richeton et al., 2005; Vinogradov et al., 2013). The combined effect of these factors leads to substantial variability in AE signals, even for test specimens and defects of similar type and size (Agletdinov et al., 2016; Zárate Boris et al., 2012). Moreover, a direct correlation between signal characteristics and defect size is often lacking (Barat et al., 2019), and a single defect may generate multiple emissions, making the definition of detection thresholds more challenging than in conventional NDT methods.

This study investigates the characteristics of AE signals generated during microblanking processes and their variation with material type, with an emphasis on distinguishing AE patterns between pristine samples and those containing pre-existing defects, such as precuts or predents. This study aims to support the development of AE-based approaches for real-time material condition classification and enhanced quality control in microshearing and microblanking processes by identifying material and condition sensitive signal features, complementing conventional post-process characterization techniques such as X-ray diffraction (XRD) and scanning electron microscopy (SEM) (Herbirowo et al., 2023). Unlike conventional AE monitoring frameworks in metal forming, which assume stable, high signal-to-noise ratio (SNR) signals and transferable spectral features, microblanking events are inherently submillisecond, strongly material-dependent, and may approach the system noise floor. Under these conditions, classical FFT-based descriptors and fixed-threshold strategies may lack robustness across different materials, highlighting the need for more resilient signal analysis methods capable of handling low-SNR transient AE signals.

2. Experimental Setup, Materials, and Methods

Several previous studies were reviewed to identify and adopt appropriate methodologies, particularly with regard to sensor placement and signal acquisition methods for cyclic signals

(Caso et al., 2023; Ferrando Chacon et al., 2015; Hidle et al., 2022; Wu et al., 2022; Zhang et al., 2020).

2.1 The AE Sensing Equipment and Microforming Machine

The sensing configuration consists of an acoustic emission sensor for real-time defect detection, a camera for visual monitoring of the forming process, and a data acquisition (DAQ) system, all of which are mounted on a 5 kN micro-forming machine, as shown in Figure 1.

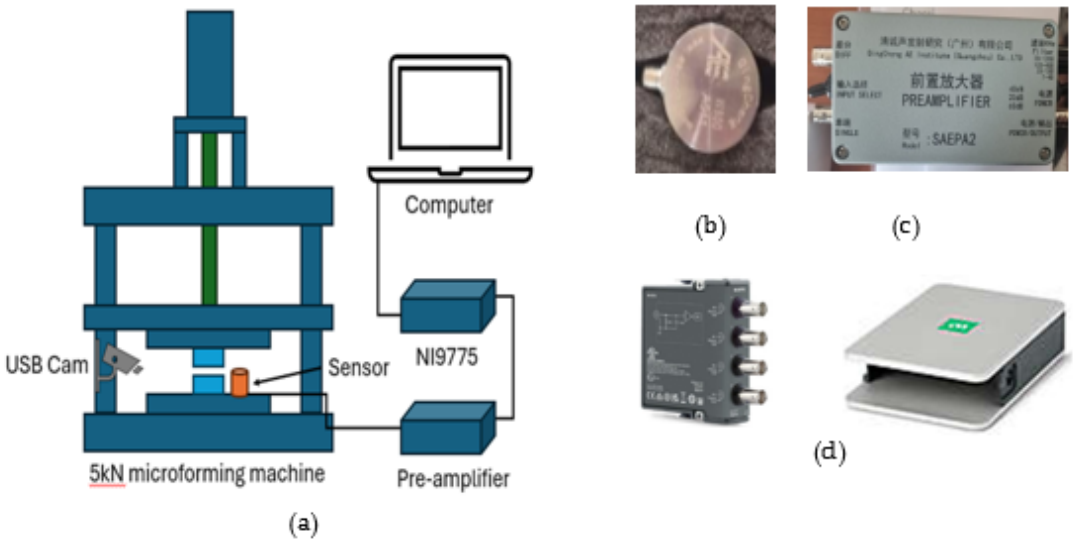

Figure 1 AE sensing system integrated with a 5 kN microforming machine: (a) schematic overview, (b) W800 sensor, (c) preamplifier, and (d) NI-9775 data acquisition module with cDAQ-9171 chassis

The 5 kN microforming machine (Kiswanto et al., 2013), as depicted in Figure 1(a), operates using an NX940MS-PS10-3 Oriental servo motor. The motor transmits mechanical force to the ram through a ball screw, converting rotational motion into linear motion. A guiding set guides the ram movement. The tooling system, consisting of punches and dies, is mounted on the upper and lower bolsters.

This study used a W800 AE sensor (Figure 1(b)) with a frequency bandwidth of 50–800 kHz and a thermal operating range of -20°C to $+80$°C. The wideband capability of the sensor is essential given the high-frequency elastic waves generated during micro-crack formation. As a piezoelectric transducer, W800 converts mechanical stress waves propagating through the forming system's steel components into electrical signals. Due to the low energy of AE signals in microscale forming processes, a signal amplifier was installed between the sensor and DAQ system to enhance signal strength and improve detectability.

As shown in Figure 1(d), the DAQ system comprises a National Instruments NI 9775 digitizer integrated with an NI cDAQ-9171 chassis, enabling high-speed data acquisition with an input range of ± 10 V and a maximum sampling rate of 20 MS/s per channel across four input channels. Connections were made using a 0.9 m, 50 Ω BNC coaxial cable, which was kept within the manufacturer's recommended limits. A fixed-gain preamplifier ensured adequate signal amplification before transmission to the acquisition system, maintaining high temporal resolution for capturing transient AE events.

The signal attenuation introduced by the measurement chain was evaluated based on the system specifications and operating bandwidth. The attenuation of the coaxial cable was estimated to be less than 0.01 dB within the analyzed frequency range below 100 kHz. The digitizer exhibited a flat frequency response well beyond the measurement bandwidth, corresponding to a Nyquist frequency of 10 MHz, resulting in negligible amplitude attenuation. The total signal

attenuation due to the cables and electronic components was estimated to be below 0.1 dB, which is insignificant relative to the measured signal levels. Because the same sensor, cable configuration, preamplifier, and acquisition parameters were consistently applied across all measurements, any systematic attenuation remained constant and did not influence the material conditions' comparative analysis.

Acoustic emission signals were acquired using a sampling rate of 2 MHz. According to the Nyquist–Shannon sampling theorem, to prevent aliasing, the sampling frequency must be at least twice the highest frequency component of the signal. Given that the effective emission bandwidth in this study was approximately 800 kHz, the theoretical minimum sampling rate was 1.6 MHz. The selected sampling rate of 2 MHz corresponds to a Nyquist frequency of 1 MHz, providing an oversampling margin relative to the dominant signal bandwidth.

A bandpass filter from 20 kHz to 1200 kHz was applied during the acquisition of the signal. With a Nyquist frequency of 1 MHz, the frequency components above this limit cannot be faithfully reconstructed. The FFT analysis of the recorded signals, plotted up to 1 MHz, showed that the dominant spectral energy was concentrated below approximately 800–900 kHz, with no significant components approaching the Nyquist frequency. Therefore, the selected sampling configuration is sufficient to capture the relevant emission characteristics without introducing aliasing. Although a higher sampling rate would further extend the Nyquist limit, the measured spectral distribution indicates that the current acquisition parameters provide adequate signal fidelity while maintaining data efficiency.

The acquired data were streamed to a connected computer for storage and subsequent offline analysis. A high-speed camera was positioned to complement the AE measurements to monitor the material during deformation, enabling synchronized visual verification of crack initiation and propagation. This study represents the first implementation of the W800 sensor in this specific micro-forming machine configuration, highlighting the importance of a wide frequency response to capture the diverse spectral characteristics of crack-induced emissions in both ductile (steel) and brittle (magnesium) materials under micro-scale forming conditions.

2.2 Materials

The experimental investigation used two primary test materials, a 0.5-mm-thick pure magnesium plate and a 0.1-mm JIS SK-5 steel sheet (comparable to SAE 1085). Table 1 summarizes the properties. These materials were selected because of their distinct mechanical characteristics and contrasting deformation responses, which are expected to influence acoustic emission signal behaviour.

Table 1 Mechanical properties of the SK-5 steel and magnesium

Material	Tensile strength (N/mm^2)	Hardness (HRC)
SK-5 steel	1570–1760	48–52
Magnesium	230–300	30–40

Initially, the experimental plan included testing multiple thicknesses (0.1, 0.2, 0.3, and 0.5 mm) for both SK-5 steel and magnesium to evaluate the effect of thickness on AE signal detectability. However, preliminary trials revealed significant limitations. Magnesium specimens thinner than 0.5 mm (e.g., 0.2 and 0.3 mm) generated weak AE signals that were difficult to detect, even when the preamplifier gain was increased to 60 dB. These signals were largely masked by noise, making them unsuitable for further investigation.

In contrast, SK-5 steel exhibited a strong AE response; even at a thickness of 0.1 mm, it produced high-amplitude signals under the lowest amplification setting (20 dB). Although thicker SK-5 sheets (0.2–0.5 mm) were initially considered, their use raised concerns regarding potential damage to the microforming dies due to the high strength and resistance to deformation of the material. Based on these considerations, the study proceeded with 0.5 mm magnesium

and 0.1 mm SK-5 steel to ensure the acquisition of clear and reliable AE signals under the given experimental constraints.

2.3 Methods

The data collection process began with the setup and calibration of the AE recording system. To ensure representative data across different structural states, test specimens were prepared under three conditions: pristine (normal/reference), precut (sheared), and predented. Measurements were repeated three times using identical parameters to ensure repeatability and statistical reliability.

Following signal acquisition, the recorded data were preprocessed and subsequently analyzed using wavelet scattering, followed by a comparative evaluation to identify differences among the material conditions. The wavelet transform provides multi-resolution analysis with adaptive time–frequency localization, enabling high time resolution at higher frequencies and low frequencies. Because the investigated signals exhibit transient and localized variations associated with dent and cut conditions, this adaptive resolution allows for the more effective characterization of such localized events. Therefore, we selected wavelet-based analysis because it offers greater flexibility in capturing subtle spectral changes across different frequency ranges.

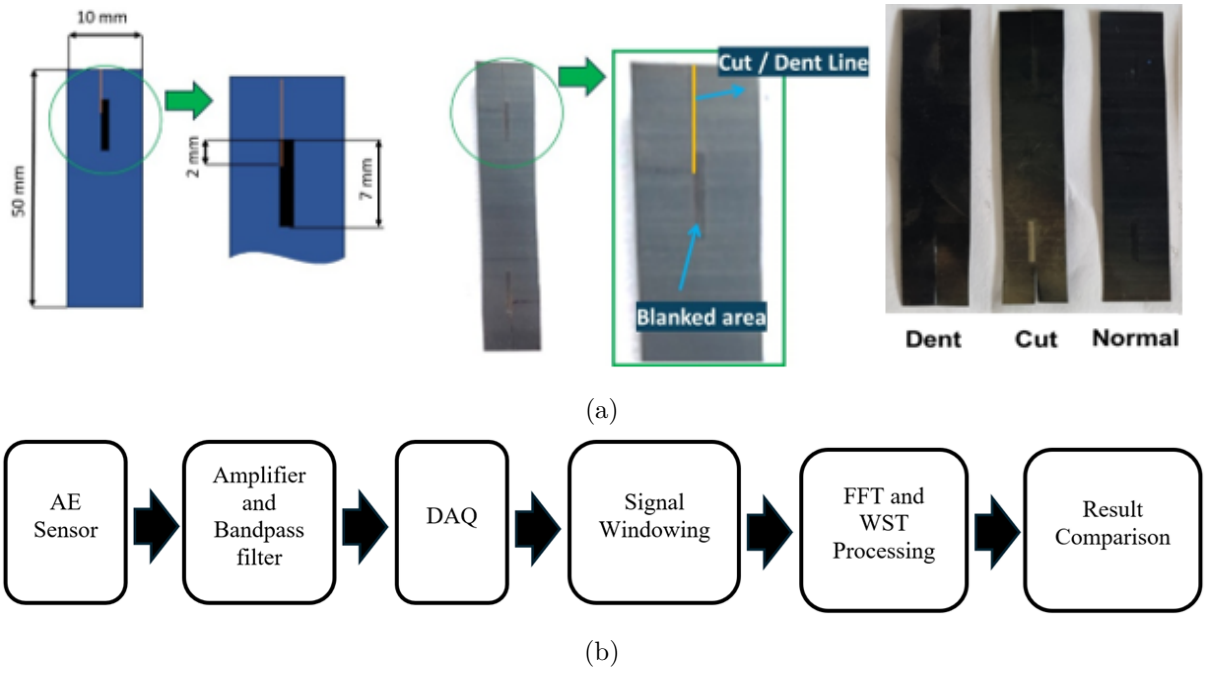

Figure 2 (a) Location of the dent and cut line on the specimen; (b) schematic workflow of AE signal processing from acquisition to comparative analysis

2.3.1 Data Acquisition

Data were acquired during the blanking of precut magnesium and SK-5 steel plate strips with dimensions of 10 mm × 50 mm. The fabricated specimens comprised pristine samples (normal material) and modified specimens incorporating precut or predent features. The precut condition simulated an initial crack that induced stress concentration, whereas the pre-dent condition represented material containing residual internal stresses from prior processing.

These defects were positioned so that they were partially overlapped by the die by 2 mm during the blanking process, as shown in Figure 2. This configuration was designed to investigate the influence of pre-existing flaws on material response under forming pressure, enabling the capture of acoustic emission signals associated with early damage initiation and deformation mechanisms. The micro-forming machine was programmed to operate in a single cycle for each

run command, with a ram speed of 6 mm/s, as shown in Figure 3.

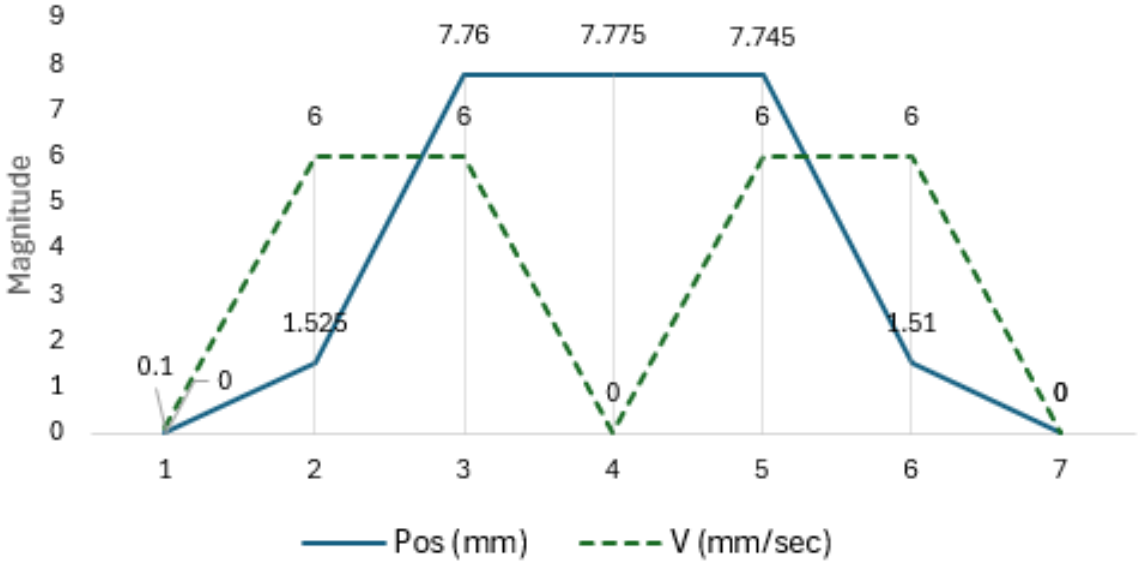

Figure 3 Operating cycle setup of the 5 kN micro-forming machine

The DAQ system was configured to record acoustic emission (AE) signals from the sensor at a sampling rate of 2 MHz. With the number of samples set to 8×10^6, a total recording duration of 4 s was obtained. Data acquisition started approximately 1 s before the forming cycle began, leaving a 2 s window corresponding to the active AE process. The sensor amplifier was equipped with a bandpass filter ranging from 20 to 1200 kHz. An amplification level of 40 dB was applied during the SK-5 steel processing, whereas 60 dB was used for the magnesium processing.

Then, the recorded data were checked and time-aligned to the predicted occurrence of the shearing process using high-speed camera recordings as the reference.

2.3.2 Wavelet Transform and Wavelet Scattering Analysis

In this study, CWT was employed to provide a time-frequency representation that captures both frequency and temporal information. The CWT is defined as:

$$W_x(a,b) = \int_{-\infty}^{\infty} x(t)\,\frac{1}{\sqrt{a}}\,\psi^*\left(\frac{t-b}{a}\right)dt \tag{1}$$

Here, $x(t)$ is the input signal, $W_x(a,b)$ is the wavelet coefficient at scale a and translation b, and $\psi^*(t)$ is the complex conjugate of the wavelet function.

In this study, the Gabor (analytic Morlet) wavelet was used, defined as follows:

$$\psi(t) = e^{-\frac{t^2}{2\sigma^2}}\,e^{i\omega_0 t} \tag{2}$$

Here, t is the time variable, σ controls the width of the Gaussian envelope, and ω_0 is the angular frequency.

3. Data Acquisition, Processing, and Analysis Results

Four-second recordings from the high-speed camera and acoustic emission sensor captured during shearing of a 0.1-mm SK-5 steel sheet were synchronized to identify the exact starting point for data segmentation (Figure 4).

Synchronization between the high-speed camera recordings and the acoustic emission signals was established using a common timestamp reference provided by the acquisition system.

In post-processing, temporal alignment was performed by correlating key mechanical events observed in the video, such as first contact and end of cut, with corresponding features in the AE waveforms, including abrupt amplitude changes. This event-based alignment defined a unified time origin for subsequent signal segmentation and analysis. The synchronization procedure provides a temporal accuracy of microseconds, minimizing potential temporal mismatches during signal subtraction and subsequent detection analysis.

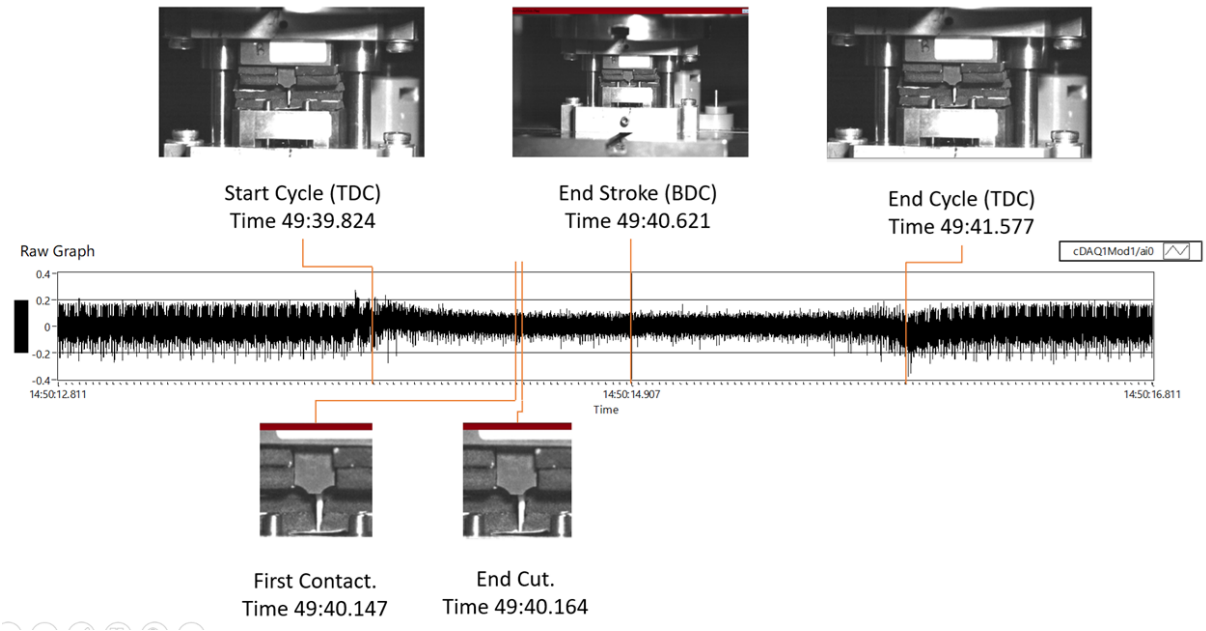

Figure 4 Synchronized AE data captured with high-speed camera recordings: (a) start of cycle, (b) end of stroke, and (c) end of cycle

Figure 5 shows the recorded data segments, each spanning up to 4 s. The recordings reveal a pronounced difference between the acoustic emission signals of SK-5 steel and magnesium, particularly in terms of signal magnitude relative to background noise. System-generated noise is evident in the results of no-load recording. Although noise reduction techniques have been reported to suppress such noise Wijaya and Kencanawati, 2014, noise cancellation was deliberately excluded from the data preprocessing stage in this study to preserve the original signal characteristics and avoid the potential loss of low-amplitude AE features relevant to early damage detection.

The 4 s AE signal was segmented into 5 ms intervals, as shown in Figure 5. Subsequently, these segments were analyzed using both FFT and WST. For the WST, the first- and second-order scattering coefficients were configured with a quality factor of 8 and 1, respectively. These parameter choices were guided by inspection of representative signals and previous studies on wavelet-based AE analysis, providing a practical balance between time–frequency resolution and feature discrimination. Although no formal preliminary sensitivity analysis was performed, these settings adequately captured both the transient and sustained components of the AE signals.

The outputs of both transforms were then compared qualitatively. For the FFT, the maximum amplitude, number of amplitude peaks, and peak frequency were considered. For the WST, the comparison focused on the frequency range, signal duration, and variations in the magnitude of the scattering coefficients (Vallen Systeme, 2013).

3.1 Fast Fourier Transform Results and Comparison

A threshold of 0.005 V was applied to the 0.1 mm SK-5 steel specimen to enable effective signal discrimination. This threshold minimized the influence of low-level noise and minor fluctuations, allowing the analysis to focus on the material response's dominant frequency com-

ponents.

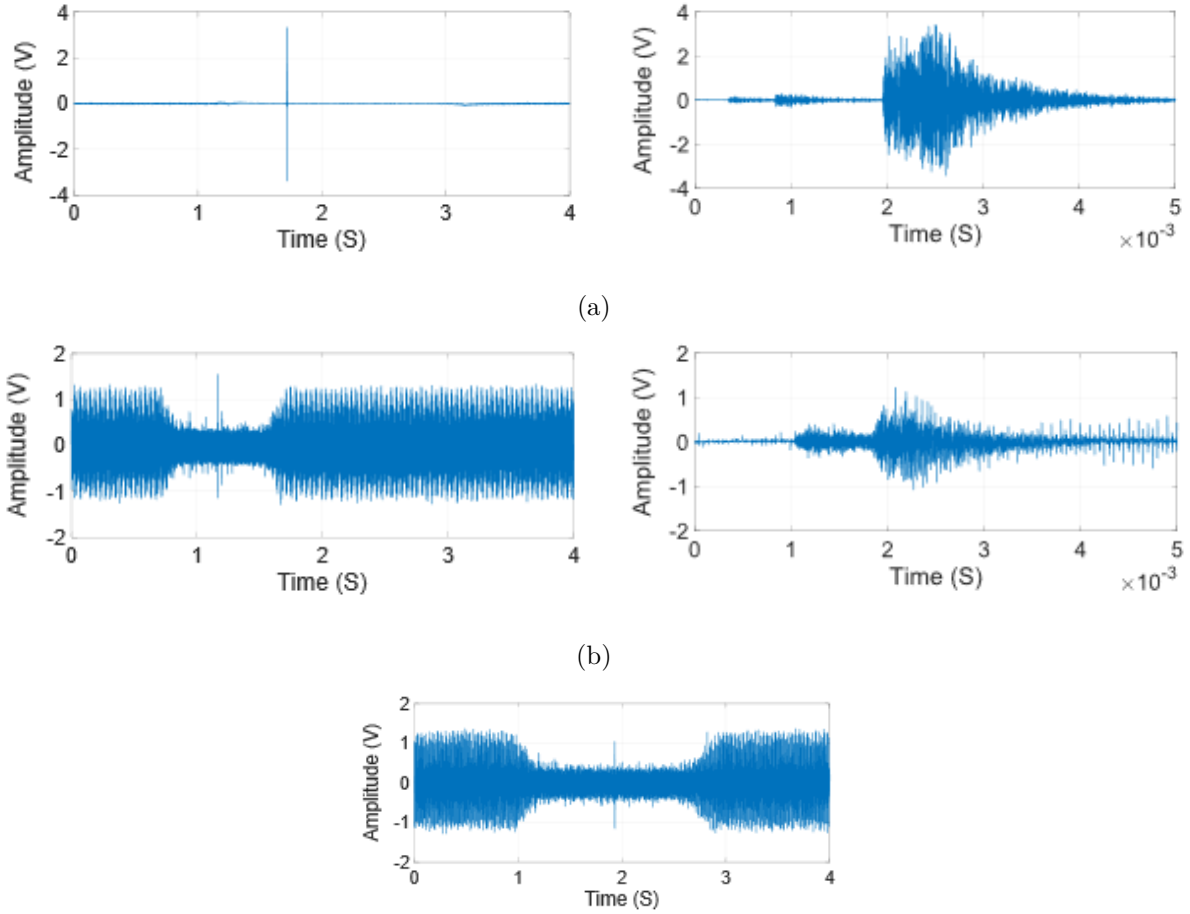

Figure 5 Sample of 4 s data record and 0.005 s segments extracted from (a) SK-5 steel, (b) magnesium, and (c) no load condition (4 s recordings only)

To further improve the visualization of the frequency spectrum behavior under different crack conditions, the signal in Figure 6 was smoothed using a Savitzky–Golay filter. The original raw signal was retained to ensure data transparency and authenticity, and a controlled denoised version was provided to facilitate clearer comparison. The Savitzky–Golay method was chosen because it effectively reduces high-frequency noise while preserving peak positions and the overall signal morphology, thereby minimizing the distortion of the intrinsic acoustic emission characteristics.

As summarized in Table 2, in the reference state, the frequency spectrum exhibited a primary amplitude peak of approximately 0.055 V. The relatively scattered peak distribution represents the inherent resonant behaviour of SK-5 steel. All amplitudes exceeding the 0.005 V threshold were considered significant contributors to the vibrational signature of the material.

Table 2 FFT results for SK-5 steel and magnesium

No.	Condition	SK-5 steel		Magnesium	
		Peak Amp ($\times 10^{-3}$ V)	SNR (dB)	Peak Amp ($\times 10^{-3}$ V)	SNR (dB)
1	Reference	55 ± 1	20.8 ± 0.2	35 ± 1	24.9 ± 0.3
2	Shear	45 ± 3	19.1 ± 0.6	40 ± 2	26.0 ± 0.4
3	Dent	40 ± 3	18.1 ± 0.7	15 ± 1	17.5 ± 0.6

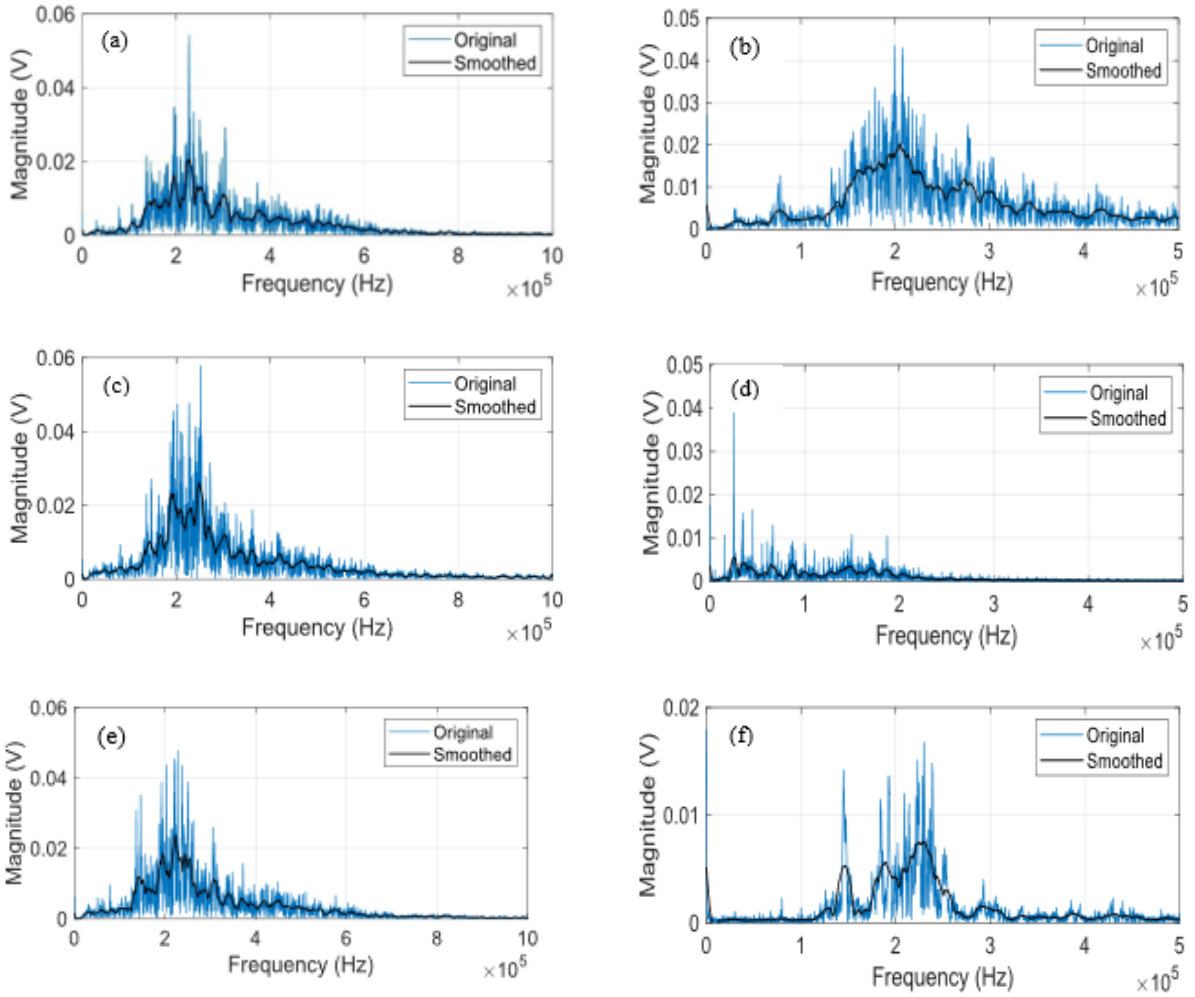

Figure 6 FFT results of AE signals recorded from SK-5 steel and magnesium under different mechanical conditions. (a–c) show the reference, shear, and dent conditions for SK-5 steel, while (d–f) show the reference, shear, and dent conditions for magnesium

During the shearing process, the main peak amplitude slightly decreased to approximately 0.045 V. However, there was a clear increase in the number of peaks above the threshold, indicating the emergence of additional frequency components. This behaviour confirms that microshearing introduces greater spectral complexity and enriches the resonance pattern due to microstructural alterations.

Under dent conditions, the principal amplitude further declined to approximately 0.040 V, accompanied by a downward shift in the dominant frequency range to 150–250 kHz. This response reflects changes in the elastic properties of the material caused by permanent deformation. Furthermore, the broadening of the spectrum below the threshold suggests increased damping and potential microstructural damage, consistent with localized plastic deformation and internal defect formation.

For the magnesium material, a threshold of 0.002 V was used for signal analysis. As summarized in Table 2, the reference (untreated) condition exhibited a maximum peak amplitude of approximately 0.035 V. The dominant frequencies ranged from 500 kHz to 1.5 MHz, as shown in Figure 6. This frequency range reflects the material's natural vibrational characteristics in its pristine state.

Following microshearing, a notable increase in peak amplitude was observed, rising to approximately 0.040 V within a higher frequency band of 1.5–2.5 MHz. Additionally, the number of frequency peaks exceeding the threshold increased significantly, indicating enhanced signal com-

plexity due to microstructural modification. This behavior suggests that the shearing process induced a richer modal vibration response and intensified resonance phenomena.

Under dent conditions, the primary amplitude peak decreased to approximately 0.015 V, while the dominant frequency shifted to a broader range of 750 kHz–1.75 MHz. The spectrum became more dispersed with reduced overall intensity, reflecting increased material damping and altered elastic properties, which may indicate the onset of internal damage.

The SNR was evaluated for all materials and deformation conditions to verify that the observed spectral variations were not influenced by background noise, as summarized in Table 2. The SNR values ranged from 18.1 to 20.8 dB for SK-5 steel and from 17.5 to 26.0 dB for magnesium, corresponding to signal amplitudes 7–20 times higher than the noise level. These values confirm that the dominant spectral components are not noise-dominated and that the FFT and WST analyses are reliable.

Notably, the magnesium signal amplitude of 0.015 V approaches the noise floor of 0.002 V under dent conditions, yielding the lowest SNR of 17.5 dB. Although this value remains within the acceptable range for spectral analysis, it represents the lower reliability limit of the present measurement system and should therefore be interpreted with caution.

3.2 Comparison of Wavelet Scattering Transform Results

Although the Fast Fourier Transform provides valuable insights into the dominant frequency components and overall spectral behaviour of AE signals under various mechanical conditions, it inherently lacks time localization and sensitivity to transient structural changes. To address these limitations and achieve a deeper understanding of the temporal evolution and hierarchical structure of the emitted signals, an advanced signal decomposition technique, namely the wavelet scattering transform, was employed.

Table 3 First-order WST results for SK-5 steel and magnesium

No.	Condition	SK-5 steel		Magnesium	
		Duration (ms)	Maximum	Duration (ms)	Maximum
1	Reference	1.5 ± 0.2	1.2 ± 0.1	2.0 ± 0.2	0.2 ± 0.05
2	Shear	0.7 ± 0.1	1.2 ± 0.1	1.2 ± 0.1	1.0 ± 0.1
3	Dent	1.0 ± 0.1	1.5 ± 0.1	1.3 ± 0.1	0.5 ± 0.05

For first-order WST results, as shown in Figure 7 and Table 3, in the reference condition, SK-5 steel exhibits higher-frequency activity in the range of 110–450 kHz, with moderate duration of ∼1.5 ms and a relatively high peak magnitude of ∼1.2, indicating stable but pronounced vibrational modes. In contrast, magnesium shows a broader low-frequency band from 50 to 225 kHz, longer sustained activity of ∼2 ms, and much lower peak magnitude of ∼0.2, reflecting the dispersed, low-energy wave propagation characteristic of its lower stiffness and higher damping.

Both materials exhibit increased spectral concentration and shorter signal duration under shear deformation. In SK-5 steel, the frequency distribution shifts slightly toward lower frequencies, accompanied by a compressed duration of approximately 0.7 ms, suggesting localized energy release. However, magnesium undergoes a pronounced shift toward higher dominant frequencies in the 150–350 kHz range, with distinct peaks between 150 and 220 kHz and a marked increase in magnitude to approximately 1.0, indicating strong transient responses and activation of high-energy deformation modes.

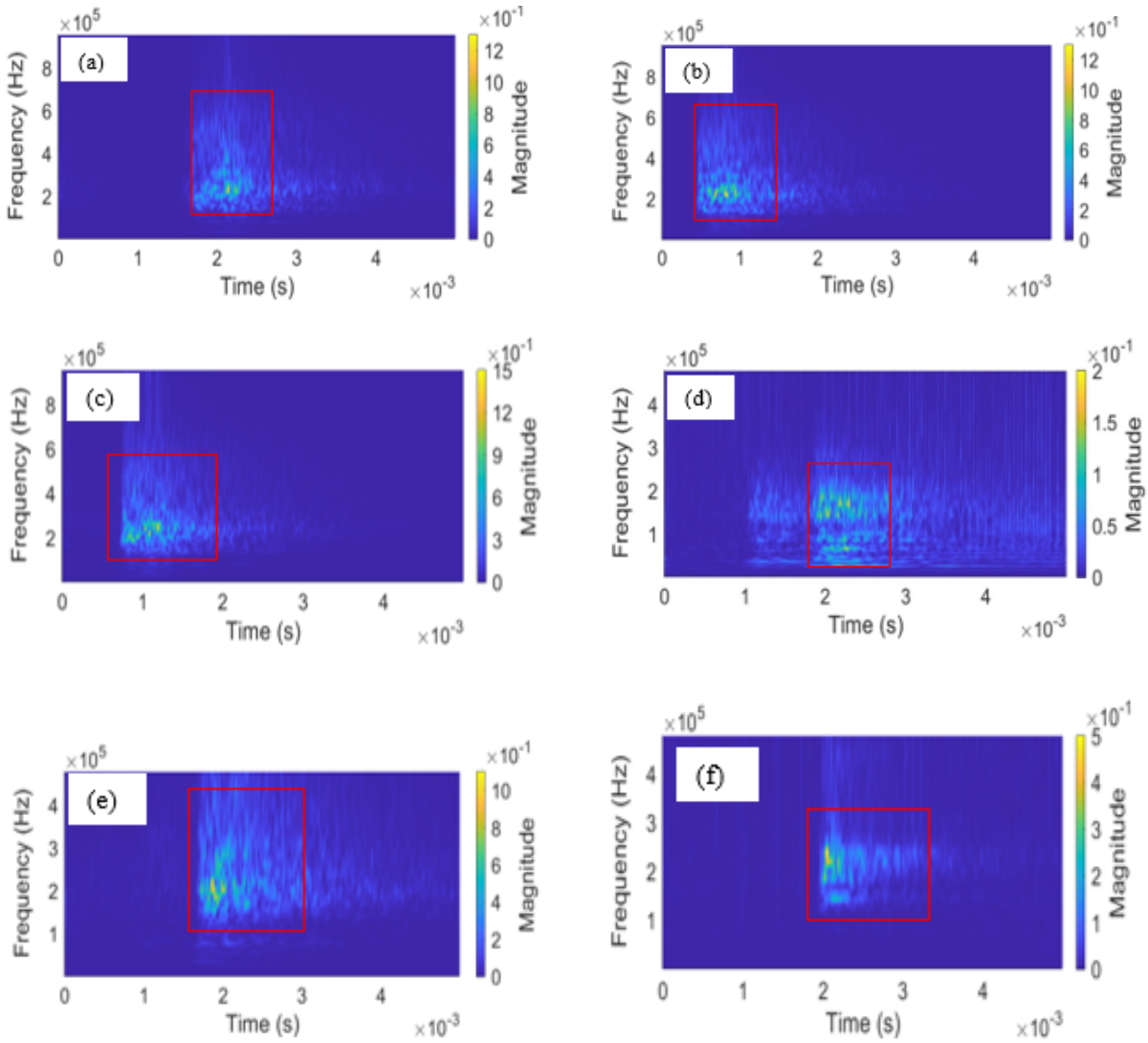

Figure 7 First-order WST results of AE data recorded for SK-5 steel 0.1 mm (a) reference, (b) shear, (c) dent, and magnesium 0.5 mm (d) reference, (e) shear, (f) dent

In the dent condition, SK-5 steel reaches its highest peak magnitude of ∼1.5 at frequencies up to 400 kHz, with a brief activity of ∼1 ms, indicating intense, localized plastic deformation. In contrast, magnesium exhibits a narrower frequency span from 120 to 280 kHz and a reduced magnitude of ∼0.5, suggesting that damping or crack closure mechanisms enhance energy dissipation. Nevertheless, finer spectral features are still observed, indicating increased signal complexity despite the lower amplitude.

Table 4 Second-order WST results for the SK-5 steel and magnesium

No.	Condition	SK-5 steel		Magnesium	
		Duration (ms)	Maximum ($\times 10^{-2}$)	Duration (ms)	Maximum ($\times 10^{-2}$)
1	Reference	0.4 ± 0.01	5.0 ± 0.5	0.5 ± 0.01	0.9 ± 0.2
2	Shear	0.6 ± 0.02	5.0 ± 0.5	0.5 ± 0.02	6.0 ± 0.5
3	Dent	0.5 ± 0.01	6.0 ± 0.5	0.2 ± 0.01	2.0 ± 0.3

The second-order WST results presented in Figure 8 and Table 4 reveal distinct nonlinear scattering behaviors between SK-5 steel and magnesium under different mechanical conditions. Under the reference state, SK-5 steel demonstrates a broader scattering range of 5–35 kHz and a

higher magnitude of 0.05, suggesting stronger multiscale interactions. This behavior is consistent with its higher elastic modulus, which may contribute to enhanced storage and release of elastic strain energy, thereby promoting nonlinear modulation effects. In contrast, magnesium exhibits a narrower scattering range of 2–15 kHz and a significantly lower magnitude of 0.009, indicating limited energy cascading and faster intrinsic attenuation. This observation is consistent with the higher damping capacity and lower stiffness of magnesium alloys.

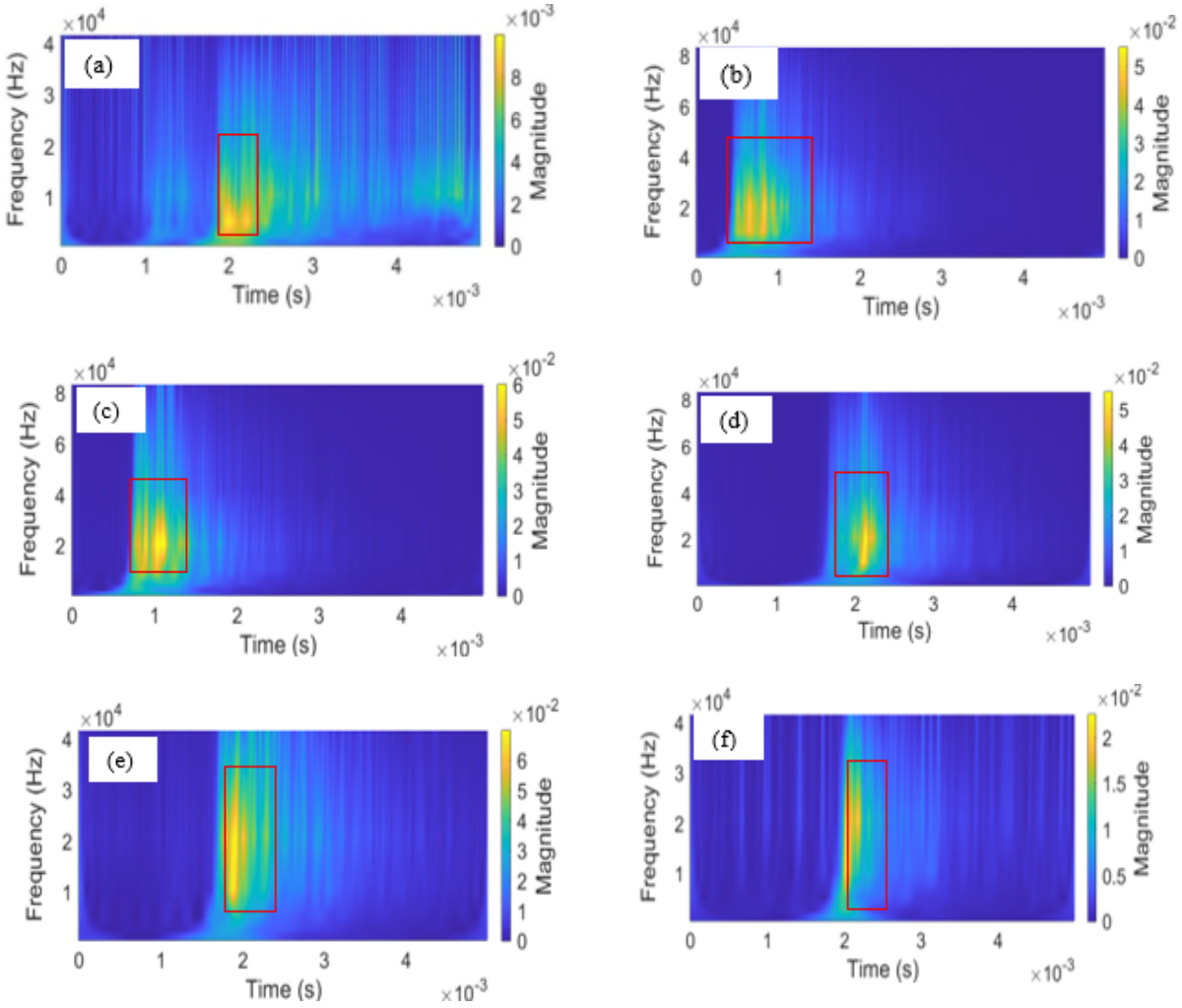

Figure 8 Second-order WST results of AE data recordings for SK-5 steel 0.1 mm (a) reference, (b) shear, (c) dent, and magnesium 0.5 mm (d) reference, (e) shear, (f) dent

Under shear deformation, SK-5 steel exhibits prolonged signal duration and slight bandwidth expansion, reflecting sustained stress redistribution and increased deformation activity. In contrast, magnesium exhibited a pronounced increase in magnitude to 0.06, indicating that shear loading activates transient nonlinear interactions, likely associated with localized slip concentration and rapid stress relaxation.

SK-5 steel reaches its maximum nonlinear response in the dent condition, which may be associated with stress concentration and potential microdamage evolution, leading to repeated wave scattering. Conversely, magnesium exhibits a shorter signal duration and lower magnitude, indicating rapid energy dissipation and limited sustained nonlinear coupling due to early attenuation and reduced elastic confinement within the material.

To contextualize these findings within the broader literature, Table 5 presents a comparative benchmark summarizing key results from previous acoustic emission studies in metallic materials, enabling direct comparison with the present results.

Table 5 Comparative benchmark of acoustic emission studies in metallic materials

Material	Experimental Condition	Analysis Method	AE Characteristics	Reference
Mg 0.5 mm	Microblanking (pristine, pre-cut, pre-dent)	FFT, WST	Short-duration, low-amplitude, transient signals	Present study
SK-5 0.1 mm	Microblanking (pristine, pre-cut, pre-dent)	FFT, WST	Stronger and more distinct transient signal	Present study
AZ31	Fatigue crack propagation	Waveform analysis, FFT	Frequency-dependent AE signals	(Han et al., 2014)
Al Alloy	Fatigue damage process	Waveform analysis	AE count rate correlated with crack propagation rate	(He et al., 2023)
A7N01	Fatigue of the base and weld	AE parameter analysis	Short bursts with moderate amplitude	(Zhu et al., 2023)

4. Conclusion and Suggestion

The AE recording method was adapted according to the mechanical properties of each material. SK-5 steel produced higher signal amplitudes at a gain of 20 dB, whereas magnesium required a higher gain of 60 dB. This confirms that the AE sensitivity is strongly dependent on the material properties. Visual observations from synchronized video recordings, supported by reference no-load signals, were essential for validating AE analysis, as FFT analysis alone was insufficient to reliably differentiate material conditions, particularly for SK-5 steel. While magnesium exhibited a clearer FFT representation due to its relatively simpler and lower-frequency dominant components, SK-5 steel showed stronger multiscale and transient characteristics, which were more effectively captured by wavelet analysis with superior time–frequency localization. First-order WST results indicated that SK-5 steel exhibited higher and more variable scattering coefficients than magnesium, reflecting more complex AE signal characteristics due to higher carbon content and greater microstructural complexity. Although shear and dent conditions influenced WST responses, the observed trends were inconclusive, highlighting the need for additional specimens or expanded experimental variables. Second-order WST analysis improved contrast and more clearly resolved patterns, particularly for image-based comparison. The resulting WST coefficient maps demonstrate strong potential for advanced analysis using two-dimensional WST or machine learning techniques. Finally, further exploration of microforming processes, combined with advanced classification approaches, such as machine learning, represents a promising direction for future work.

Acknowledgements

This research was funded by the Indonesian Ministry of Education, Culture, Research, and Technology (Kemendikbudristek) through the Doctoral Dissertation Research Grant (NKB-1145/UN2.RST/HKP.05.00/2023).

Conflict of Interest

The authors declare no conflicts of interest.

References

Abdollahi-Mamoudan, F., Ibarra-Castanedo, C., & Maldague, X. P. V. (2025). Non-destructive testing and evaluation of hybrid and advanced structures: A comprehensive review of methods, applications, and emerging trends. *Sensors*, *25*, 3635. https://doi.org/10.3390/s25123635

Agletdinov, E., Pomponi, E., Merson, D., & Vinogradov, A. (2016). A novel Bayesian approach to acoustic emission data analysis. *Ultrasonics*, *72*, 89–94. https://doi.org/10.1016/j.ultras.2016.07.014

Alcaraz, J. Y., Sharma, A., & Tjahjowidodo, T. (2024). Predicting porosity in wire arc additive manufacturing (WAAM) using wavelet scattering networks and sparse principal component analysis. *Welding in the World*, *68*, 843–853. https://doi.org/10.1007/s40194-024-01709-5

Al-Jumaili, S. K., Eaton, M. J., Holford, K. M., Pearson, M. R., Crivelli, D., & Pullin, R. (2018). Characterisation of fatigue damage in composites using an Acoustic Emission Parameter Correction Technique. *Composites Part B: Engineering*, *151*, 237–244. https://doi.org/10.1016/j.compositesb.2018.06.020

Allwood, J. M., Ashby, M. F., Gutowski, T. G., & Worrell, E. (2013). Material efficiency: Providing material services with less material production. *Philosophical Transactions of the Royal Society A*, *371*, 20120496. https://doi.org/10.1098/rsta.2012.0496

Altan, T., & Tekkaya, A. E. (2012). Classification and description of sheet metal forming operations. In *Sheet metal forming: Fundamentals*. ASM International.

Barat, V., Marchenkov, A., & Elizarov, S. (2019). Estimation of fatigue crack AE emissivity based on the Palmer–Heald model. *Applied Sciences*, *9*(22). https://doi.org/10.3390/app9224851

Barile, C., Casavola, C., Pappalettera, G., & Kannan, V. P. (2020). Application of different acoustic emission descriptors in damage assessment of fiber reinforced plastics: A comprehensive review. *Engineering Fracture Mechanics*, *235*(107083). https://doi.org/10.1016/j.engfracmech.2020.107083

Caso, E., Fernandez-Del-Rincon, A., Garcia, P., Diez-Ibarbia, A., & Sanchez-Espiga, J. (2023). An experimental study of acoustic emissions from active surface degradation in planetary gears. *Mechanical Systems and Signal Processing*, *189*. https://doi.org/10.1016/j.ymssp.2022.110090

Dwiyati, S. T., Kiswanto, G., & Supriadi, S. (2025). Development of a room-temperature microforming process applied to pure magnesium treated by annealing in bioabsorbable miniplate implant applications. *Results in Engineering*, *27*. https://doi.org/10.1016/j.rineng.2025.107051

Ferrando Chacon, J. L., Kappatos, V., Balachandran, W., & Gan, T. H. (2015). A novel approach for incipient defect detection in rolling bearings using acoustic emission technique. *Applied Acoustics*, *89*, 88–100. https://doi.org/10.1016/j.apacoust.2014.09.002

Ghassemali, E., Tan, M. J., Jarfors, A., & Lim, S. (2012). Progressive microforming process: Towards the mass production of micro-parts using sheet metal. *The International Journal of Advanced Manufacturing Technology*, *66*, 611–621. https://doi.org/10.1007/s00170-012-4352-4

Han, Z., Luo, H., Sun, C., Li, J., Papaelias, M., & Davis, C. (2014). Acoustic emission study of fatigue crack propagation in extruded AZ31 magnesium alloy. *Materials Science and Engineering: A*, *597*, 270–278. https://doi.org/10.1016/j.msea.2013.12.083

He, X., Yan, Z., Liang, H., & Wang, D. (2023). Corrosion fatigue acoustic emission characteristics and evaluation of friction stir welding joints of AZ31 magnesium alloy in 3.5 wt.% NaCl solution. *Journal of Materials Research and Technology*, *25*, 4582–4594. https://doi.org/10.1016/j.jmrt.2023.06.240

Herbirowo, S., Yuwono, A. H., Sofyan, N., Imaduddin, A., Pramono, A. W., Supriyadi, S., & Mohamed, J. J. (2023). Development of magnesium diboride superconducting wires through

hot working with different initial filling density. *International Journal of Technology*, *14*. https://doi.org/10.14716/ijtech.v14i7.6695

Hidle, E. L., Hestmo, R. H., Adsen, O. S., Lange, H., & Vinogradov, A. (2022). Early detection of subsurface fatigue cracks in rolling element bearings by the knowledge-based analysis of acoustic emission. *Sensors*, *22*. https://doi.org/10.3390/s22145187

Ingarao, G., Di Lorenzo, R., & Micari, F. (2011). Sustainability issues in sheet metal forming processes: An overview. *Journal of Cleaner Production*, *19*, 337–347. https://doi.org/10.1016/j.jclepro.2010.10.005

Kiswanto, G., Mahmudah, A., & Supriadi, S. (2013). Development and testing of 5 kN micro forming machine for micro part manufacturing. *13th Quality in Research*, 84.

Kumar, P., Maiti, J., & Gunasekaran, A. (2018). Impact of quality management systems on firm performance. *International Journal of Quality & Reliability Management*, *35*, 1034–1059.

Li, H., & Fu, M. (2019). *Deformation-based processing of materials: Behavior, performance, modeling, and control*. Elsevier.

Linderov, M., Segel, C., Weidner, A., Biermann, H., & Vinogradov, A. (2014). Deformation mechanisms in austenitic TRIP/TWIP steels at room and elevated temperature investigated by acoustic emission and scanning electron microscopy. *Materials Science and Engineering: A*, *597*, 183–193. https://doi.org/10.1016/j.msea.2013.12.094

Ma, J., Tang, X., Hou, Y., Li, H., Lin, J., & Fu, M. W. (2025). Defects in metal-forming: Formation mechanism, prediction and avoidance. *International Journal of Machine Tools and Manufacture*, *207*. https://doi.org/10.1016/j.ijmachtools.2025.104268

Mu, W., Gao, Y., Wang, Y., Liu, G., & Hu, H. (2022). Modeling and analysis of acoustic emission generated by fatigue cracking. *Sensors*, *22*. https://doi.org/10.3390/s22031208

Nurcahyo, R., Wibowo, A. D., Robasa, R., & Cahyati, I. (2019). Development of a strategic manufacturing plan from a resource-based perspective. *International Journal of Technology*, *10*. https://doi.org/10.14716/ijtech.v10i1.2140

Ono, K. (2005). Current understanding of mechanisms of acoustic emission. *The Journal of Strain Analysis for Engineering Design*, *40*, 1–15. https://doi.org/10.1243/030932405X7674

Richeton, T., Weiss, J., & Louchet, F. (2005). Dislocation avalanches: Role of temperature, grain size and strain hardening. *Acta Materialia*, *53*, 4463–4471. https://doi.org/10.1016/j.actamat.2005.06.007

Seleznev, M., Gustmann, T., Friebel, J. M., Peuker, U. A., Kühn, U., Hufenbach, J. K., Biermann, H., & Weidner, A. (2022). In situ detection of cracks during laser powder bed fusion using acoustic emission monitoring. *Additive Manufacturing Letters*, *3*. https://doi.org/10.1016/j.addlet.2022.100099

Shiraiwa, T., Tamura, K., & Enoki, M. (2019). Analysis of kinking and twinning behavior in extruded Mg–Y–Zn alloys by acoustic emission method with supervised machine learning technique. *Materials Science and Engineering: A*, *768*, 138473. https://doi.org/10.1016/j.msea.2019.138473

Sutherland, J. W., Skerlos, S. J., Haapala, K. R., Cooper, D., Zhao, F., & Huang, A. (2020). Industrial sustainability: Reviewing the past and envisioning the future. *Journal of Manufacturing Science and Engineering*, *142*, 110806.

Twardowski, P., Tabaszewski, M., Wiciak-Pikuła, M., & Felusiak-Czyryca, A. (2021). Identification of tool wear using acoustic emission signal and machine learning methods. *Precision Engineering*, *72*, 738–744. https://doi.org/10.1016/j.precisioneng.2021.07.019

Unterberg, M., Voights, H., Weiser, I. F., Feuerhack, A., Trauth, D., & Bergs, T. (2021). Wear monitoring in fine blanking processes using feature based analysis of acoustic emission signals. *Procedia CIRP*, *104*, 164–169. https://doi.org/10.1016/j.procir.2021.11.028

Vallen Systeme. (2013). Codes, standards, practices, and guidelines related to acoustic emission (AE).

Vinogradov, A., Lazarev, A., Linderov, M., Weidner, A., & Biermann, H. (2013). Kinetics of deformation processes in high-alloyed cast transformation-induced plasticity/twinning-induced plasticity steels determined by acoustic emission and scanning electron microscopy: Influence of austenite stability on deformation mechanisms. *Acta Materialia*, *61*, 2434–2449. https://doi.org/10.1016/j.actamat.2013.01.016

Wang, S. B., Yan, Z. F., Zhang, H. X., He, X. L., Dong, P., Wang, W. X., & Wang, Z. R. (2022). Acoustic and thermal energy evolution of AZ31B magnesium alloy under static tensile deformation. *Journal of Materials Research and Technology*, *20*, 1645–1658. https://doi.org/10.1016/j.jmrt.2022.07.169

Wijaya, I. G. P. S., & Kencanawati, N. N. (2014). Denoising acoustic emission signal using wavelet transforms for determining the micro crack location inside of concrete. *International Journal of Technology*, *5*, 259–268. https://doi.org/10.14716/ijtech.v5i3.613

Wu, L., Liang, W., & Sha, D. (2022). A novel adaptive noise reduction method for field natural gas pipeline defect detection signals. *International Journal of Pressure Vessels and Piping*, *199*, 104761. https://doi.org/10.1016/j.ijpvp.2022.104761

Xu, K., Lyu, J., & Manoochehri, S. (2022). In situ process monitoring using acoustic emission and laser scanning techniques based on machine learning models. *Journal of Manufacturing Processes*, *84*, 357–374. https://doi.org/10.1016/j.jmapro.2022.10.002

Zárate Boris, A., Caicedo Juan, M., Yu, J., & Ziehl, P. (2012). Probabilistic prognosis of fatigue crack growth using acoustic emission data. *Journal of Engineering Mechanics*, *138*, 1101–1111. https://doi.org/10.1061/(ASCE)EM.1943-7889.0000414

Zhang, H., & Lin, Z. (2023). Analytical solution of acoustic emission in soft material with cracks by using reciprocity theorem. *Engineering Fracture Mechanics*, *277*. https://doi.org/10.1016/j.engfracmech.2022.108996

Zhang, X., Wang, K., Wang, Y., Shen, Y., & Hu, H. (2020). Rail crack detection using acoustic emission technique by joint optimization noise clustering and time window feature detection. *Applied Acoustics*, *160*, 107141. https://doi.org/10.1016/j.apacoust.2019.107141

Zhu, R., Fang, S., Sun, W., & Chi, D. (2023). Study on acoustic emission characteristics of fatigue damage of A7N01 aluminum alloy for high-speed trains. *Materials*, *16*, 4362. https://doi.org/10.3390/ma16124362